Guiding lunar growth: architectural solutions for space traffic management

Michael Bilka
BAE Systems, Space and Mission Systems
Raymond Wright and Joshua Wysack
BAE Systems, Space and Mission Systems

ABSTRACT

As human exploration returns to the Moon with the intent of establishing a permanent presence, infrastructure capabilities that are multi-service and scalable are required for a self-sustaining lunar economy. These activities will see growing lunar traffic to include landing, relaunches, and low-orbiting vehicles. The expected increase in future lunar traffic requires coordination of trajectories and operations of spacecraft travelling to, from, and around the Moon as well as surface launches. A system is needed to monitor future lunar traffic, which will require a combined architecture of observers on the lunar surface and space-based observers.

The major architecture trades and estimated performance of a lunar Space Traffic Management (STM) architecture leveraging Lunar Surface Observatory (LSO) and Low Lunar Orbit (LLO) observers are presented. These two architecture components can perform complimentary roles in providing traffic management near the Moon. Space-based systems offer several advantages, including dynamic viewing geometries and ability to look up or down, but may suffer from stray light and surface clutter issues when viewing near the lunar surface. Ground-based sensors have the advantage of viewing along the lunar surface to detect landing or launch of objects but suffer from the power challenges of the lunar night. Architecture trades include number and location of observers, both ground and space, in this combined architecture. The analysis will demonstrate coverage of lunar orbiters and sample descent trajectories based on historic missions.

1. Introduction

The last decade has seen an increased interest in returning to the Moon for science and exploration along with an increase in space faring nations with lunar exploration capabilities. NASA, for example, has a long-term roadmap with the Artemis missions. This roadmap includes science missions as well as manned lunar spacecraft for landing and crewed Gateway missions [1].

Beyond science, interest in lunar exploration is expected increase due to assessments of the potential future lunar economic zone, which has inspired not just governments but commercial industry as well. Reference [2] assessed the potential economic market space with respect to three categories: Transportation, lunar data, and resource utilization (e.g. mining). The outcome projected a $170 billion market up to 2040 – pending the continued growth towards technology maturation and international cooperation (e.g. treaties, shared policy). This kind of economic incentive has an impact on the commercial space landscape and, as of 2020, nearly 100 companies across 11 countries have plans to offer services and products on the Moon or in cislunar space [3]. **Fig. 1**, reproduced from [3], shows the commercial service/market activity as a function of number of offering companies, color coded by country of origin. This indicates a wide, global interest in the future lunar economy and the increase in space faring nations, as compared to the early lunar exploration era of the 1960's-1970's.

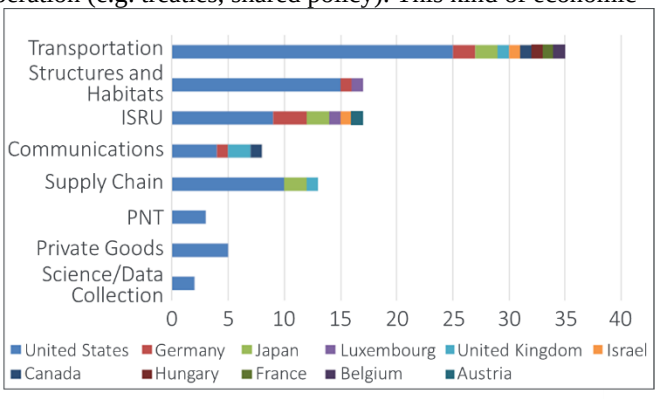

Fig. 1. Potential Future Lunar Commercial Enterprise Activities as a function of Country of Origin; reproduced from [3]

Infrastructure will be needed to support this future potential, and research is underway across the community to address the future infrastructure of the lunar environment, for

example [1] [4] [5]. Along with transportation, major infrastructure needs include communications and lunar surface power to support lunar exploration and commercial economic activities.

Lunar space traffic management will become a necessity for the lunar economic zone to reach its full potential. A recent report from the Korea Pathfinder Lunar Orbiter (KPLO) mission operations [6] showed 41 collision alerts over 71 days in 2023 with the current level of traffic! This is shown in **Fig. 2**, reproduced from [6], with alert instance and vehicle alert pairs as a function of the assessed time period. To ensure safety and availability to all, lunar space traffic management is needed to manage current and future traffic growth.

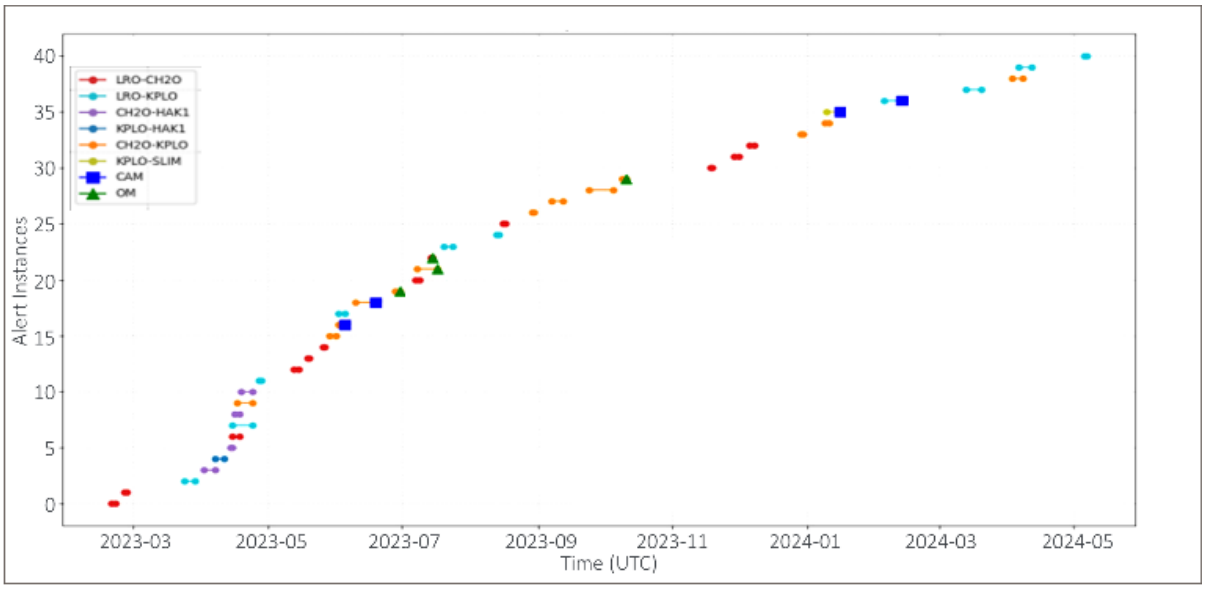

Fig. 2. Duration of collision reports between spacecraft as reported from KAA; reproduced from (1)

Lunar Space Traffic Management is differentiated from Space Situational Awareness (SSA) and is defined here as the technical and regulatory provisions to support safe access to the lunar and cislunar space [7] – hence it is expected to be a cooperative activity for all nations, similar to air traffic control. In the present work, this definition is leveraged to develop an architecture to meet Lunar Space Traffic Management (STM) needs in an assumed regulatory bounded environment.

Lunar surface and Low Lunar Orbiting (LLO) space is very difficult to observe from long-range sensors because of lunar straylight and surface clutter for transiting spacecraft, requiring technologies that can look 'across and out' to maintain safety of flight. An STM architecture is developed leveraging scalable, passive EO sensing approaches. The STM OV-1 is shown in **Fig. 3**. The space segment of the Lunar STM architecture is designed for surveillance of lunar orbiters, arrival, and departure from lunar orbit. It is assumed to have the sensor/vehicles occupying equally space orbital planes, shown as the blue orbital curves. The space segment offers capability of dynamic viewing geometries but may suffer from stray light from the Luner limb when viewing near the surface. The ground segment is designed to monitor ascent and descent trajectories for lunar landers and lower orbit trajectory and offers the capability to view along the Lunar surface.

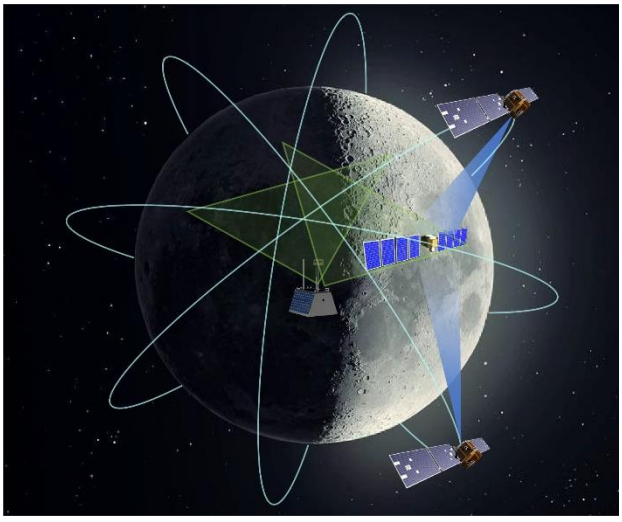

Fig. 3. OV-1 Lunar Space Traffic Management system comprised of ground and space based sensing

2. Approach

The STM architecture is divided into a space segment and ground segment to provide the best coverage for orbiting and landing traffic. This architecture is intended to leverage the strengths and capabilities of lunar orbiting space vehicles (ability to efficiently search large volumes) and ground systems (better low altitude coverage due to lunar stray light) to meet STM coverage needs. The architecture is based on the BAE systems previously published hybrid space senor for Space Domain Awareness [8] and Lunar Surface Observatory (LSO) [9] & [10].

The individual sensor performance is tabulated in **Table 1**. The space sensor has a narrow Field of View (FOV) combined with high agility with a visual magnitude providing a viewable range of 93,000 km of an assumed 1m diameter target at SNR of 6. Comparatively, the ground sensor leverages a wide FOV optical design for a fixed sensor direction and a 9.8 visual magnitude for a visible range of 2,0000 km, also assuming a 1m diameter target and SNR of 6. The reduced range is due to the sensitivity reduction caused by the WFOV. The ground segment is the most limiting performance but provides sufficient range coverage to account for low orbiting traffic and landing conditions that may not be observable by the space segment due to lunar stray light.

Table 1. Space and Ground Sensor Parameters used to model architecture performance.

Parameters	Space Sensor	Ground Sensor - Fixed
visual magnitude (mv)	16.8	9.8
FOV	2 x 4 deg	100° & 120° cone
Slew rate & accel	3 deg/s & 3 deg/s^2	fixed
Detectable range @ best solar phase*	93,200 km	2,000 km

The analysis is segmented by defining the STM volume of responsibility between 20km and 10,000km from the lunar surface, divided between a space segment and a ground segment and delineating at 2,000km. This is illustrated in **Fig. 4**, showing the relative volume responsibilities for the grounds segment (blue) and space segment (white). Each segment is optimized independently and the results define the total combined architecture.

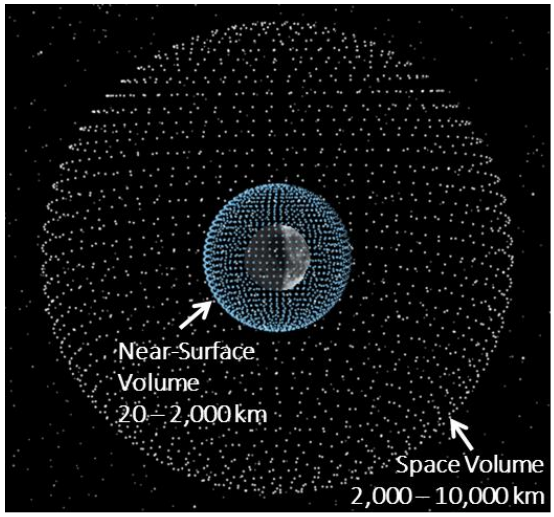

Fig. 4. Lunar STM volumes. Near surface – launch and landing coverage from ground sensors, Space volume -arrival and departure STM from Space System

Architecture optimization is framed around a reference mission of observing a trajectory through approach and landing at the lunar south pole. An example is shown in **Fig. 5** which shows the Chandrayaan-3 trajectory and decent to the lunar surface as a function of time [hours]. The trajectory is broken into segments, labeled for ease of discussion – these labels are not intended to provide a formal definition set on any or all landing trajectories. The dashed line is placed at 2,000 km to illustrate which system I intended to provide the primary tracking during the trajectory. The transit phase is the end of the Earth to Moon trajectory that enters lunar orbit and the space segment area of responsibility (10,000 km). It begins its lunar orbital trajectory resulting in the staging phase. The staging phase, in this instance, is an elliptical orbit that is transitioning between the ground and space segments area of responsibilities (at 2,000 km). The orbit is circularized at the start of the approach phase as the spacecraft prepares for final maneuvering toward landing.

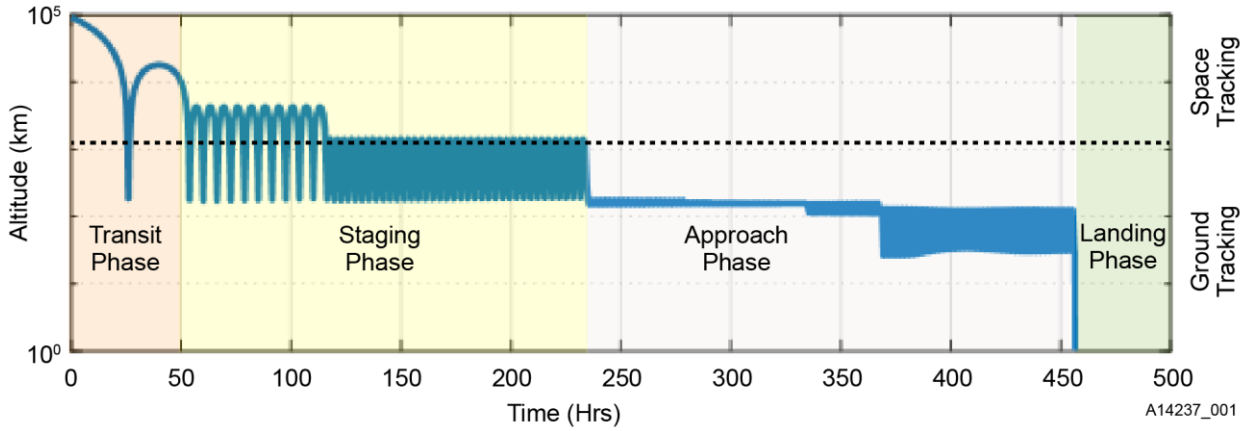

Fig. 5. Chandrayaan-3 trajectory from entry into lunar orbit through landing. Sequence is divided into arbitrary phases for ease of discussion.

Space Segment Architecture

The space segment performance is simulated using software developed at BAE as part of an AMOS 2022 paper [11]. This software uses capacity analysis within a scheduling optimization algorithm to provide optimal coverage results for a constellation of sensors working collaboratively. These results are used to assess the search capability and determine the optimum architecture. The simulation parameters include the sensor parameters listed in **Table 1**, a one-meter target with reflectance of 0.2, solar exclusion angle of 30° half angle from the center, and Earth and Moon exclusion angles of 5° from the limb. The sensor integration time is taken to maximize search capability and is selected based on achieving the minimum sensor Signal-to-Noise Ratio (SNR) of six. SNR is shown as a function of commanded integration time for the space sensor in **Fig. 6**, with the SNR of six crossing highlighted.

The space segment architecture performance is assessed via two coverage metrics. Observability analysis assesses the line-of-sight coverage as a percentage of search volume, constrained by solar phase angle and celestial body exclusions. Capacity analysis expands observability by including the individual sensor FOV and agility. Capacity analysis also includes the collaboration of multiple sensors to assess percentage coverage of the search volume. The search volume is discretized into points for the volume search grid (**Fig. 4**). The calculated capacity, as a percentage of the search volume, is given by **Eq. 1**. Over each time step the number of observed points ($pObs_{t_n}$) is summed for all sensors in the architecture and is normalized by the total number of discretized points in the volume (T_v).

$$\boldsymbol{Capacity}\ (\boldsymbol{t_n})\% = \mathbf{100} \times \frac{\sum_0^{t_n} \boldsymbol{pObs_{t_n}}}{\boldsymbol{T_v}} \quad \textbf{(1)}$$

The calculation of percent capacity then results in a curve that shows the sum total observations in the given search volume as a function of time. Given a fixed search time, capacity is used to determine the best sensor arrangement to perform a volume search.

For the purposes of this investigation, each sensor of the space segment is assumed to be in circular orbits of equally spaced orbital planes with 86° inclination. With this constraint and the fixed search

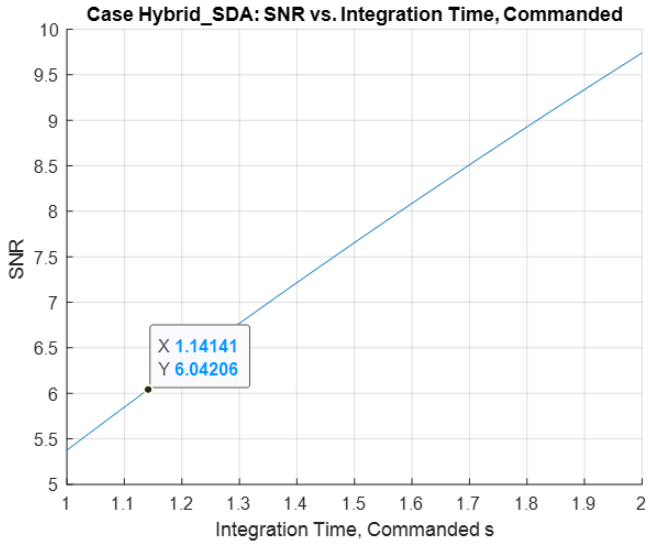

Fig. 6. SNR as a function of commanded integration time for the space sensor – SNR 6 crossing emphasized.

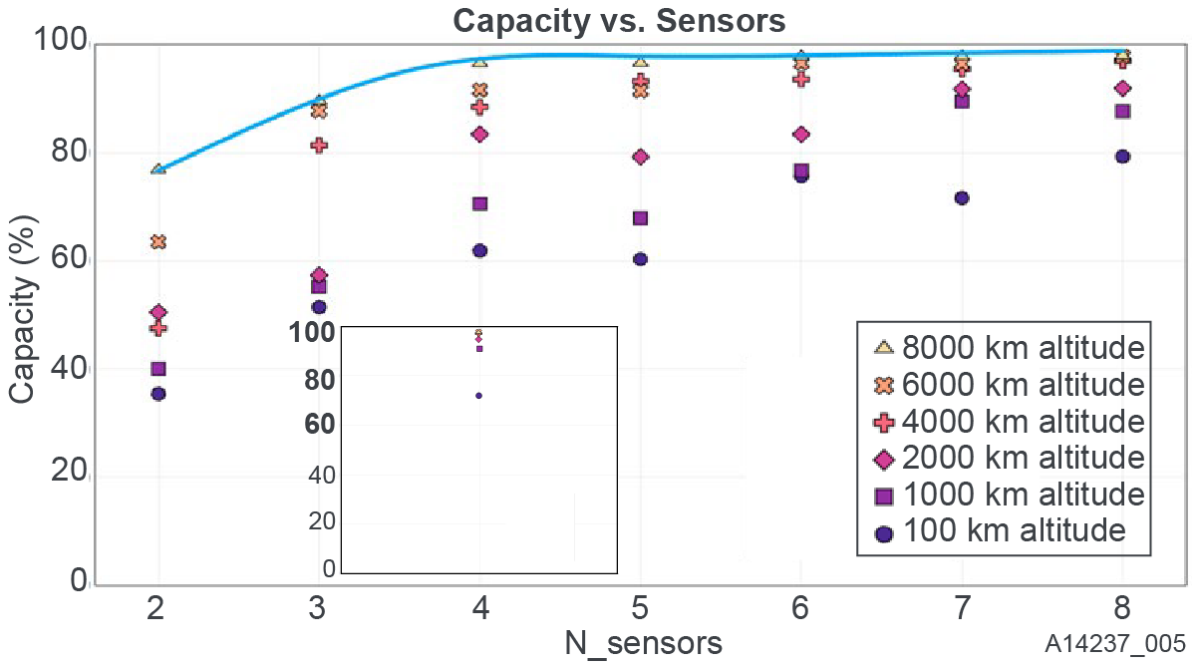

Fig. 7. Capacity percentage as a function of space sensor quantity and altitude – inset is analysis of 4 space sensors with the radiometric inputs for present work.

volume extending from 2,000 km to 10, 000 km, the architecture is optimized against orbital altitude and number of sensors. The best solution minimizes the number of required space sensors while maximizing the capacity percentage of the architecture.

Analysis has been previously made for optimization of a space senor search system that is leveraged as a starting point. Space sensor capacity is evaluated for orbital altitudes from 100 km through 8,0000 km and for up to eight sensors (orbital planes). The results of this analysis are summarized in **Fig. 7.** The figure shows maximum capacity percentage for all configurations as a function of sensor quantity and altitude. This analysis imposes a search time limit of six hours (roughly equivalent to one circular orbital period at 2,000 km) to achieve an asymptote for the max value of each configuration. Note: it is not expected for any configuration to reach 100% capacity due to exclusions. It is shown that the maximum search capacity increases with increasing sensor orbital altitude across all instances of sensor quantity. Evaluating sensor quantity against the 8,000 km altitude shows that the capacity reaches an asymptotic value of approximately 97% for a four-sensor architecture, with diminishing returns for increased sensor quantity. Inset to **Fig. 7** shows the capacity for the four sensor architecture as a function of altitude using the radiometry and boundary conditions for the current sensor analysis. It is shown to have the same trend, although with somewhat different maximum capacity values per altitude. The maximum capacity is still the 8,000 km altitude sensors configuration at 98%. It would not be expected to improve with additional sensors in a significant way.

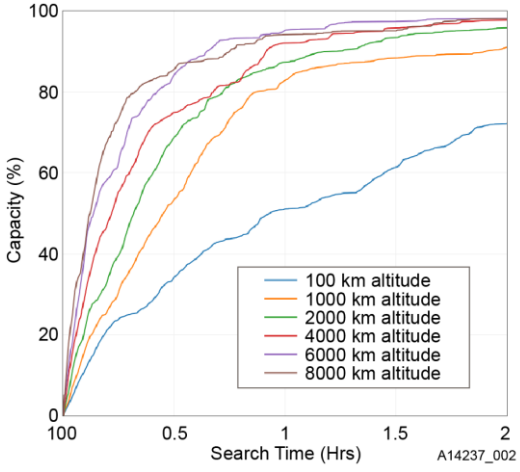

Fig. 8. Four sensor space segment capacity percentage as a function of search time, limited to two hours, and senor orbital altitude.

The STM space segment is expected to be able to quickly identify traffic entering the space volume of responsibility. **Fig. 8** shows the capacity percentage as a function of time for a four sensor architecture at different altitudes from 100 km – 8,000km, limited to a two hour search. This is use to estimate the best time response architecture – in this case the defined requirement of 90% capacity. What is observed in the data is

that maximum capacity over the search window is reached in less time with increasing altitude. Interestingly, with respect to responsiveness of the architecture, the initial slope of the capacity percentage is greater with increasing altitude as well. That is, the higher the orbital altitude of the search sensors results in large volumes searched in the short time from the search start. For example, the 8,000 km orbit altitude architecture can capture 70% of the volume in the first 20 minutes compared to less then 30% for the 100 km orbit altitude architecture. Setting a search capacity threshold of 90%, it is shown that the 6,000 km altitude architecture reaches it the fastest, achieving it in ~40 minutes, with 8,000 km not far behind at ~44 minutes.

For the given lunar space segment search volume, the selected space architecture consists of four sensors placed on equally space orbital planes at an 86° inclination. While the 6,000 km reached the 90% capacity threshold in the least amount of search time, 8,000 km orbital altitude is selected for the final architecture. This is justified as the threshold is met in a similar time frame but the 8,000 km orbital altitude also had the larger initial slope – maximizing initial search response in the shortest time.

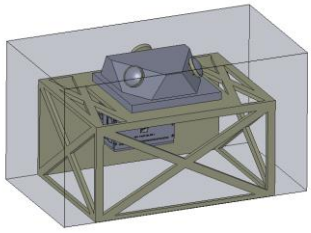

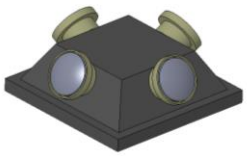

Fig. 9. Example LSO architecture. Left shows a lightweighted packaging with the three sensor head, with 120° angular spacing. Right: Four sensor head with 90° angular spacing.

Ground Architecture

The ground segment is based on the previously published Lunar Surface Observatory (LSO). In the previous study each LSO was equipped with a single Wide Field of View (WFOV) sensor looking directly up. For the Lunar STM ground segment, a multi sensor architecture is considered, where each LSO may have three sensors (120° cone) or four sensors (100° cone). The WFOV sensors are used to provide broad coverage of low orbits and passing transit trajectories. An example of an LSO architecture is shown in **Fig. 9**, illustrating a lightweighted chassis and two multi-sensor head architectures for three and four sensors. The sensors have an angular separation of 120° and 90° for the three and four sensor configurations respectively. The vertical tilt of the sensors is such that the projection of the WFOV cone on a plane cut through center and perpendicular to the lunar surface has the bottom edge parallel to the surface – "looking across."

The sensors are arranged along lunar equator to support observation of low altitude trajectories with respect to the south pole lunar lander reference mission. The LSOs are equidistantly spaced along the equator and four and eight LSO system emplacements are analyzed for the Lunar STM ground segment performance. One LSO is assumed to be at the south pole landing area to monitor descent. The equatorial configurations are shown in **Fig. 10**. Qualitatively, there appear to be larger gaps in coverage for the four sensor ground architecture (left) that become closed when the LSO quantity is doubled (right). Quantitative performance metrics are needed to optimize the architecture- maximizing capability while minimizing quantity of systems.

The LSO architectures are fixed observers and a different optimization metric is needed to quantify performance – search capacity having little meaning for a system that is not 'searching'. The ground segment performance is quantified against ability to observe orbiting trajectories within the ground volume area of responsibility. Two orbits are applied for the analyses, a circular polar orbit and a 60° inclined circular orbit for the target trajectory. Each target orbit is evaluated at 100, 1,000, and 1,800 km altitudes. The architectures performance is assessed against gaps in coverage for these target trajectories.

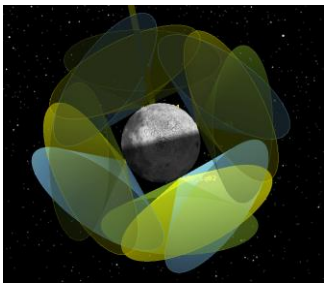

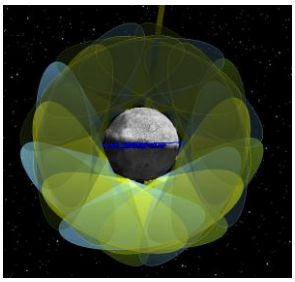

Fig. 10. Visual illustration of equidistant, equatorial placement of LSO systems – 3 sensor architecture used for illustrative purposes only. Left – 4 LSO systems; Right 8 LSO systems

All other LSO system components being the same, there is a reduction in sensitivity due to the change in FOV (cone angle) for the differing configurations. This is quantified in **Fig. 11** where the SNR is shown as a function of range and sensor FOV. At the 2,000 km range limit

for the LSO sensors, the SNR for the 100° cone meets the minimum SNR value of 6, whereas the 120° cone SNR is reduced to 4. This analysis combined with the greater coverage volume enabled by the four sensor architecture eliminates the three sensor configuration from further analysis herein.

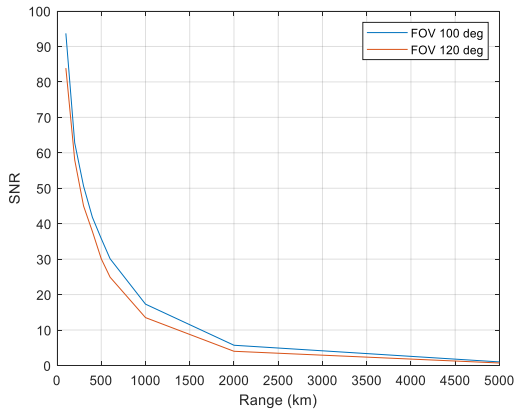

Fig. 11. SNR as a function of range and FOV cone angle for individual LSO senor – 120° 3 sensor architecture, 100° 4 sensor architecture.

Performance for the ground segment with the four sensor component LSO is evaluated by quantifying the maximum coverage gap and the frequency of the gaps in coverage. This performance is simulated in STK for the LSO systems and target orbits described previously. The target observations as a function of time are calculated. A requirement of one observation per orbit is assumed and gaps are defined when this is not met. A sample output is shown in **Fig. 12** where the time between target observations normalized by the target orbital period is shown as a function of the total observation window of one month for a target at a 1,000 km polar orbit. Within the figure the max gap is defined as the occurrence of maximum gap in observation to any LSO sensor- this result is averaged for comparison between configurations.

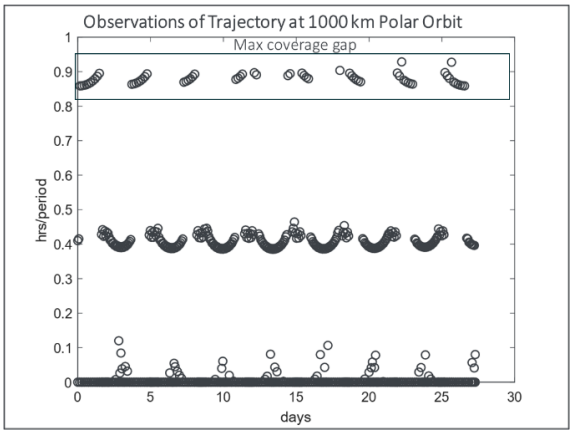

Fig. 12. Observations of reference 1000km Polar Orbit trajectory for 8 LSO configuration. Observation time, normalized by orbital period shown as a function of orbit pass for one month in days. Max gap in observations and frequency of gap is illustrated for reference.

Comparison is made between a ground segment architecture consisting of four and eight equally spaced LSO systems along the Moon's equator. A sampling of the results for the circular polar orbit is shown in **Table 2**. A full set of simulations was also conducted for the 60° inclined orbit targets. The analysis showed a similar trend in the analysis of the coverage gaps and only the polar orbit data is shown for brevity. For both the four and eight LSO ground architectures the analysis shows worse coverage – larger gaps with more frequent occurrences for targets at the 100 km orbit, although significantly worse for the 4 LSO arrangement. The coverage significantly improves for targets at 1000 km orbits for both as well. The system performance appeared to be worse for target altitudes that approached the altitude limit for the ground search volume. For both the 100 km and 1,800km orbits the gaps are the result of reduced sensor overlaps between LSOs at those altitudes, which becomes a periodic occurrence as a function of the orbital procession.

Table 2. Observation Performance Comparison of 4 and 8 equidistantly spaced equatorial LSO emplacements; Green includes analysis with the fours space sensor included.

Target Orbit	Orbital Period (hrs.)	Avg. max gap (hours/period)
8 LSO systems		
100 km polar	1.96	5.55
1000 km polar	3.57	0.88
1800 km polar	5.24	11.7
1800 km polar + 4 space sensors	5..24	0.35
4 LSO systems		
100 km polar	1.96	45.55
1000 km polar	3.57	11.96

The gap behavior is illustrated in **Fig. 13** for a 100 km polar orbit with the eight LSO ground segment and showing the orbital procession (blue lines) with respect to the LSO coverage and gaps. Five-to-six orbital periods are seen in the 'triangular' coverage gap, which is consistent with the max gap for this orbit shown in **Table 2.**

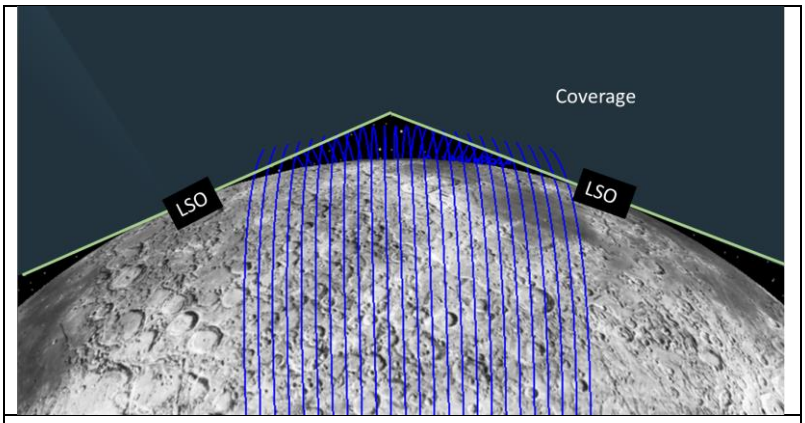

Fig. 13. Illustration of coverage gaps due to orbital procession for 100 km polar orbit

One of the objectives is to minimize number of sensors for the system. For long staging and approach times, the larger coverage gaps at higher altitudes could have little impact for traffic management, however, may impact shorter duration trajectories. Given the significantly worse performance of the 4 LSO system at 100 km and 1000 km altitude, nearly 46 orbital periods without coverage, the 8 LSO architecture is selected as the baseline.

3. Architecture Performance

The best assessed architectures from the space and ground segment individual optimized analysis are combined for the total Lunar Space Traffic Management system. The final components of the architecture are shown in **Fig. 14**. The left picture illustrates (blue orbital lines) the optimized space architecture with four space sensors on equally spaced orbital planes at 86° inclination and orbital altitude of 8,000 km. The middle picture illustrates the coverage for the ground segment with an 8 Lunar Surface Observatory architecture with a four sensor configuration, equally spaced along the lunar equator. An initial assessment of performance is conducted by including the space segment in the 1,800 km polar orbit target trajectory simulation. This result is shown in **Table 2** and highlighted in green. This shows an order of magnitude improvement in coverage for the target trajectory. Illustrating the increased observation capability of the combined system.

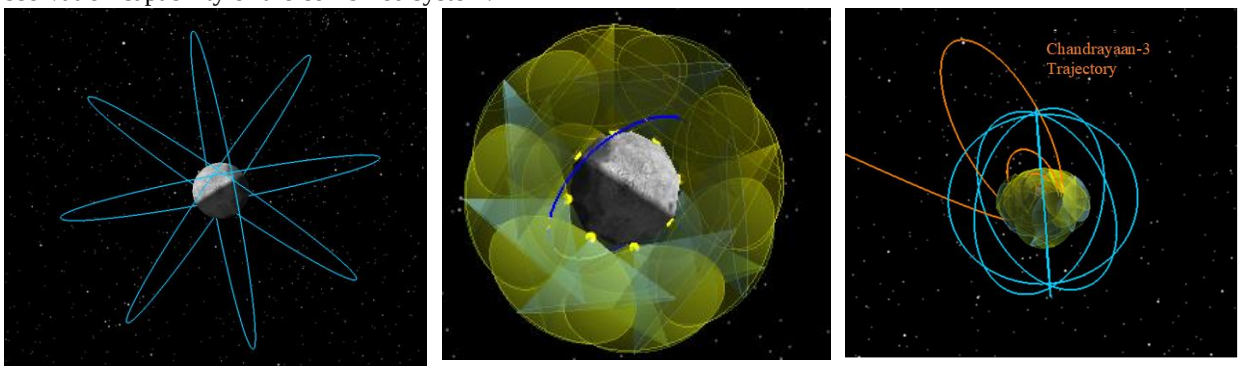

Fig. 14. Final optimized lunar Space Traffic Management Architecture. Left: orbital planes for 4 space segment sensors. Middle: 8 LSO systems with four sensors each, equidistantly placed at the lunar equator; Right. Combined STM architecture illustrating coverage of the Chandrayaan-3 landing trajectory (orange)

The complete STM architecture is evaluated against historical approach and landing trajectories. For illustrative context, the combined Lunar STM architecture is shown with the Chandrayaan-3 orbit and landing trajectory in **Fig. 14** on the right. The initial transit and staging phase of the trajectory with respect to the STM system is seen.

The combined architecture is evaluated against the observability of the Chandrayaan-3 orbit and landing sequence through simulation. The Chandrayaan-3 trajectory provides a good test case for this architecture capability with its eccentric orbits and stair stepping down in altitude during its landing sequence. Coverage of the trajectory is demonstrated in **Fig. 16.** The Chandrayaan-3 trajectory altitude is shown as a function of time with the horizontal dashed line representing the separation of the ground and space volume of responsibility at 2,000 km. For clarity,

sections of the staging and approach conditions of the trajectory are magnified with observations color coded for the STM observers. The black line is the Chandrayaan-3 trajectory. The blue-green line is the portion of the trajectory that is observed by the space segment and the red line is the portion of the trajectory that is observed by the ground segment. The space segment can observe to an altitude lower than the defined 2,000 km volume boundary. Combined with the ground architecture the staging phase is well covered throughout that phase of the trajectory. With the drop in altitude for the approach phase, the trajectory is only observable with the ground segment. However, the trajectory is still able to be observed by an LSO nearly once per target revolution around the moon. A similar simulation is conducted for the IM-1 lander trajectory, shown in **Fig. 17.** The IM-1 trajectory is a shorter duration then Chandrayaan-3 and rapidly reaches an altitude where only the ground system can make observations. While the coverage of the space segment is not shown, it is able to capture the rapid descent of the transit phase down to 3,000 km. The ground segment can make 1-2 observations per lunar revolution. The number of observations per trajectory are tabulated by mission (Chnadrayaan-3; IM-1) and altitude range and are shown in **Fig. 15.**

Mission	Altitude Range	# Obs/rev
IM-1	0-200 km	2
IM-1	2k – 10k km	Constant above 3k km
Ch3	20 – 140 km	3, 1
Ch3	110 – 160 km	3
Ch3	150 – 170 km	1 – 3
Ch3	200 – 1,400 km	½ rev
Ch3	2,000 – 4,200 km	½ rev
Ch3	4k – 10k km	Constant

Fig. 15. Tabulated results of historical lander trajectories vs STM architecture observations.

4. Conclusions and Future Work

In this paper we investigated a Lunar Space Traffic Management architecture leveraging a scalable approach for ground and space based sensing systems. The architecture is designed around a reference mission of trajectory and landing targeting the lunar south pole. The ground and space segments are analyzed separately with the best outcomes for each segment combined to provide the total STM architecture. The total architecture is assessed against historic known trajectories, Chandrayaan-3 and IM-1. It is found that the architecture provides regular observations throughout the entire trajectory from transit through landing.

The analysis showed that while the space segment of the architecture could provide observations at lower altitude than the expected boundary for the space volume of responsibility, the ground segment is needed for observations of

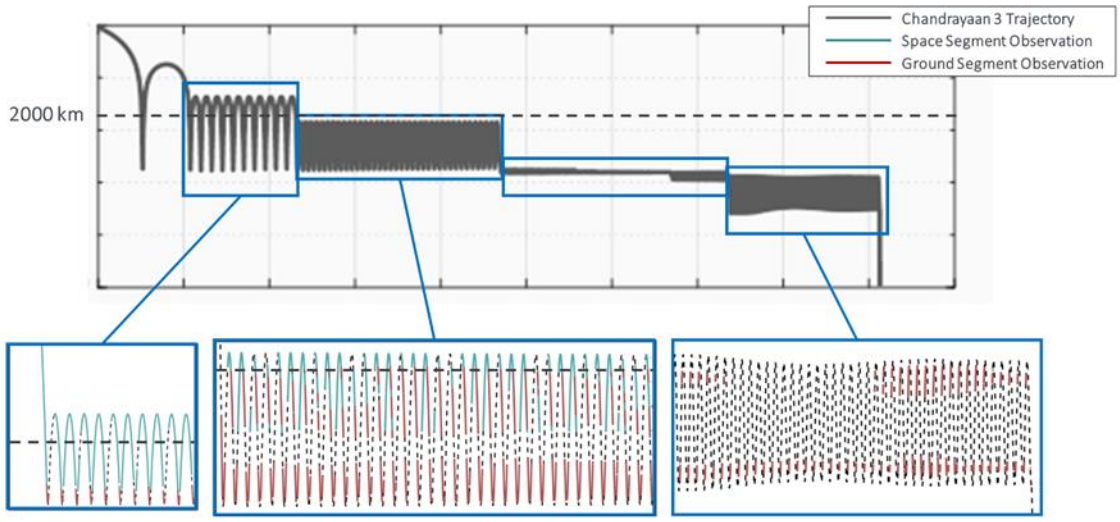

Fig. 16. Observability of the Chandrayaan-3 lander trajectory from the combined Lunar Space Traffic Management architecture. Black line illustrates the Chandrayaan-3 trajectory as a function of altitude and time. Blue-green line illustrates observation from the space segment. Red line illustrates observations from ground segment.

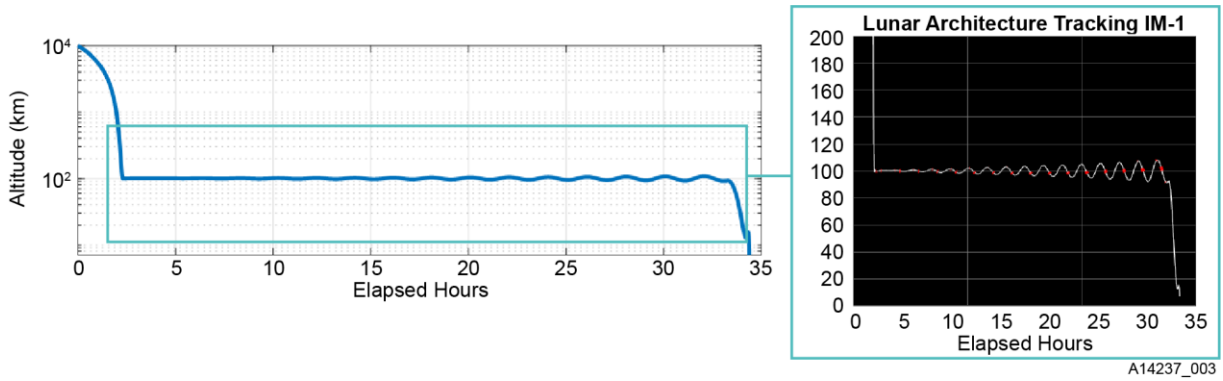

Fig. 17. Observability of the IM-1 lander trajectory from the combined Lunar Space Traffic Management Architecture. Blue line is the IM-1 trajectory. Red overlay are the observations of the ground segment of the architecture.

lower orbits. Attempts to lower the altitude of the space architecture may decrease the observation altitude limit but comes at the expense of decreasing the search capacity of the space system – a critical metric to ensure optimal coverage of transiting spacecraft. The ground architecture provides limited observations capability due to the fixed LSO emplacement, but when strategically placed can provide valuable observations for the reference mission trajectories.

Future work could expand on the architecture optimization through optimization steps that include the space and ground segments. It is shown that the ability of the space segment to observe the target trajectories beyond the lower limit of the bounding volume supported a minimization of the needed ground segment systems. A future analysis could include this while also optimizing the orbit altitude of the space architecture to compliment the ground architecture. These observation outputs could then be used to assess against flight plans to better understand needed fidelity for a lunar STM like the one proposed. Additional investigations could be made at the ground component system level to assess Size, Weight and Power constraints and optimize based on potential power needs and availability (e.g. future lunar power systems).

References

1. Csank, Jeffrey. *Sustainable Power for the Lunar Surface*, Interagency Advanced Power Group, 2021.
2. Scatteia, Luigi and Perrot, Yann. *Lunar Market Assessment: market trends and challanges in the development of a lunar economy*, s.l. : PwC, 2021.
3. Colvin, Thomas, et al. *Deman Drivers of the Lunar and Cislunar Economy*, IDA Science and Technology Institute, Washington, DC, 2022.
4. Csank, Jeffrey, et al. *Powering the Moon: From Artemis Technology Demonstrations to a Lunar Economy*, Nuclear and Emerging Technolgies for Space, 2022.
5. Thomas, George, et al. *Establishing a Lunar Surface Power Grid*, Conference on Advanced Power Systems for Deep Space Exploration, 2022.
6. Jeon, Moon-Jin. *Lessons learned for Safe and Sustainable Lunar Exploration: The Case of the KPLO Operations*, 67th session of the Commitee on the Peaceful Uses of Outer Space, Vienne : s.n., 2023.
7. Madi, M and Sokolova, O, [ed.]. *Space Debris Peril: Pathways to Opportunities*, CRC Press, Boca Raton, 2021.
8. Lawitzke, Anna, et al. *Hybrid Sensor for Joint Space Domain Awareness and Lunar Surface Intelligence*, Advanced Maui Optical Space Surveillance Technologies Conference, Maui : s.n., 2022.
9. Van Cleve, Jeffrey, Lawitzke, Anna and MacAnlis, E. *Hiding in plain sight: observing objects in low lunar orbit and the L2 dark cone from a lunar surface observatory*, Advanced Maui Optical and Space Surveillance Technologies Conference, Maui : s.n., 2021.
10. Van Cleve, Jeffrey, et al. *A year in the life of the Shackleton space domain awareness station*, Advanced Maui Optical and Space Surveillance Technologies Conference, Maui : s.n., 2022.
11. Owens-Fahrner, Naomi, Correa, Jeremy and Wysack, Joshua. *Capacity-based Cislunar Space Domain Awareness Architecture Optimization*, Advanced Maui Optical and Space Surveillance Technologies Conference, Maui : s.n., 2022.